Journal of Asian Concrete Federation
Vol. 3, No. 2, pp. 82-89, December 2017
ISSN 2465-7964 / eISSN 2465-7972
https://doi.org/10.18702/acf.2017.12.3.2.82

Technical Paper

Research on flexural behavior of the externally prestressed UHPC box girder

Jiazhan SU*; Renyuan DU; Baochun CHEN; and Qingwei HUANG

(Received: July 15, 2017; Accepted: November 14, 2017; Published online: January 5, 2018)

Abstract: Experiment on an externally prestressed ultra high performance concrete (UHPC) box girder subjected to symmetrical concentric loads is carried out. The behavior of the test girder is investigated, including the load-deflection curve at mid-span, cracking pattern, strain distribution, and failure mode. The mid-span nominal moment capacity of the girder is analyzed. Test results show that the anti-cracking capacity of UHPC box girder is better than that of a normal prestressed concrete (PC) girder. The tensile property of UHPC should be taken into account in the process of calculating mid-span nominal moment capacity of the externally prestressed UHPC box girder. Finite element (FE) model analysis results agree well with the test results. The influencing parameter, concrete grades, was studied numerically to compare the flexural behavior of UHPC girder with PC girder. The cracking moment and ultimate load calculation method is proposed, which can meet precision for engineering practice and can be a reference method for design calculation of a prestressed UHPC box girder.

Keywords: flexural behaviour, UHPC, external prestressing, box girder, test, calculation method.

1. Introduction

Ultra High Performance Concrete (UHPC) is a relatively new type of concrete which has higher strength, greater stiffness, and better durability than normal concrete and high-performance concrete. It is mainly composed of cement, silica fume, sand, super-plasticizer, and steel fiber [1]. It has a broad application prospects in civil engineering, including bridges, buildings, nuclear engineering, municipal structures, ocean engineering, due to its different roles in reducing the structural self-weight, enhancing the bearing capacity, and improving the ductility [2,3]. At present, the UHPC box girder had been used for bridges in Japan [4], Austria [5,6], and Malaysia [7,8]. Compared to I-shaped or T-shaped girders, the box girders offer better resistance to torsion, which is particularly of benefit if the bridge deck is curved in plan. Additionally, larger girders can be constructed, because the presence of two webs allows wider and hence stronger flanges to be used. However, experimental investigation has focused on I-shaped and T-shaped girders [9,10], few researches have to do with prestressed UHPC box girders, and few test results are available on the UHPC girders. Therefore, the mechanical behavior of large-scale UHPC box girder is required by engineering and it is necessary to carry out an investigation.

Corresponding author Jiazhan SU is an assistant professor of College of Civil Engineering, Fuzhou University, China.
Renyuan DU is an assistant professor of School of Civil Engineering and Architecture, East China Jiaotong University, Nanchang, China.
Baochun CHEN is a professor of College of Civil Engineering, Fuzhou University, China.
Qingwei HUANG is an associate professor of College of Civil Engineering, Fuzhou University, China.

2. Experimental programme

Taking a trial design UHPC foot-bridge as the prototype [11], the UHPC box girder model was a quarter of size of the original one. The total length of the test girder was 12.4 m (see Fig. 1). The test girder was simply supported at both ends with a span of 12.0 m. The girder was made up of five precast segments connected by wet joints cast-in-situ (200-mm-thick). Six shear keys were set on two webs at joint section of segment for improving the shear capacity at the connection of segments. The profile and reinforcement of a segment is shown in Fig. 2. The height of the segment is 400 mm. The width of the top and bottom flanges is 1,250 mm and 600 mm, respectively. The top and bottom flanges and two webs have the same thickness of 50 mm. A total of 15 and 7 steel bars with 8-mm diameter were used at the top flange and the bottom flange, respectively, while ten 6-mm diameter steel bars were used in the webs. Two 15.2-mm diameter

steel strands were set as external tendons and 200-mm width deviators were set for external tendons.

The mix proportion of UHPC used for the girder was as follows: 842.4 kg/m^3 ordinary Portland cement, 985.6 kg/m^3 sand taken from Minjiang River with particle size less than 0.63 mm, 252.7 kg/m^3 silica fume in which the content of SiO_2 was more than 90%, and 156 kg/m^3 micro steel fibers with length of 13 mm and diameter of 0.22 mm and tensile strength of 2,850 MPa. In order to match the material properties of the precast UHPC and the cast-in-situ UHPC, the steel fiber volume content of wet joint UHPC was 3%, higher than that of the precast concrete (2%). The water-to-binder (the cementitious materials include cement and silica fume) ratio was 0.18 and 21.1 kg/m^3 poly carboxylic high-performance super-plasticizer was used to improve the workability of the UHPC mixture. The test girder was cured in natural environment for 2 days, and then in steam environment (180ºC) for 8 hours, and then left in natural environment for 14 days. Wet joints were cured in 100ºC steam chamber for 3 days in-place.

The mechanical properties of the UHPC are given in Table 1, where f_{cc} is the compressive strength measured on 150 mm × 150 mm × 150 mm cubes, f_{ck} is the prism (150 mm × 150 mm × 300 mm) compressive strength, f_t is the flexural tensile strength, E_c is the Young modulus. The mechanical properties of reinforcing steel bars are listed in Table 2.

The loads were located in third span points symmetrically as shown in Fig. 1. The central region between the two loads was subjected to constant bending moment with zero shear. Strain gauges were positioned at $L/2$, $L/4$, $3L/4$, two loading points, and bearing sections to measure the strains of reinforcing steel and UHPC. Seven linear variable displacement transducers (LVDTs) were set at the same positions to measure the displacement of the girder. The test photograph is shown in Fig. 3.

Table 1 – Material properties of UHPC

Item	f_{cc} (MPa)	f_{ck} (MPa)	f_t (MPa)	E_c (MPa)
Precast segments	160.0	150.0	8.01	4.16×10^4
Wet joints	150.4	140.4	9.18	4.05×10^4

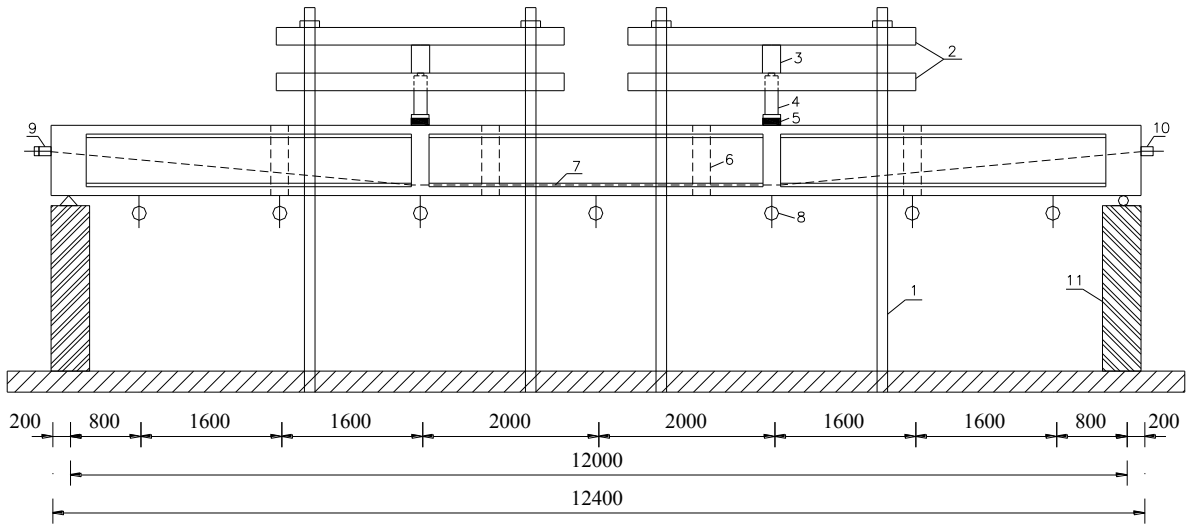

1—anchored shaft; 2—longitudinal reaction beam; 3—lateral reaction beam; 4—hydraulic jack; 5—rubber cushion block; 6—joint; 7—external tendon; 8—linear variable displacement transducers; 9—fixing anchorage device; 10—tension anchorage device; 11—steel bearing platform

Fig. 1 – Test setup for the model (unit: mm)

Table 2 – Material properties of reinforcing steel

	Yield strength (MPa)	Ultimate tensile strength (MPa)	Modulus of elasticity (MPa)
Normal steel bars	359	460	1.97×10^5
Steel strands	1,603	1,886	1.94×10^5

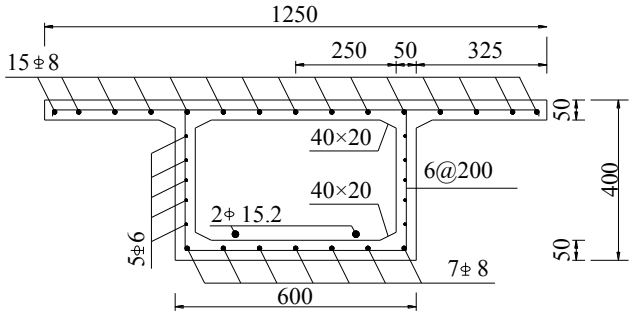

Fig. 2 – Profile and reinforcement of the cross-section (unit: mm)

Fig. 3 – Test set-up

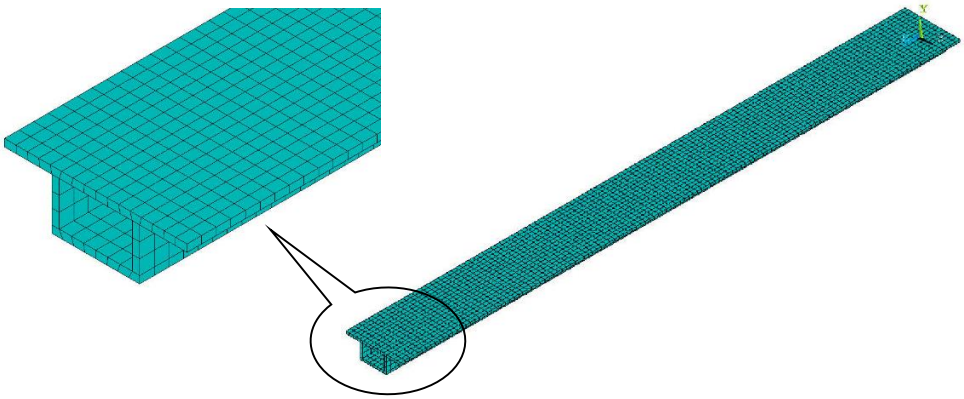

Fig. 4 – FEM of the model girder

3. FE model

For further studying of the flexural behaviour of UHPC girder, the finite element program, ANSYS, was used for 3-D analyses of UHPC girder. The objectives of the analysis were to explain the discrepancies of experimental results, and to enhance the understanding of the accuracy of the theoretical assumptions for the problems. Throughout the studies, the concrete was modeled using solid element, Solid65. The 8-node solid element with 24 DOF is capable of modeling cracking and crushing of concrete. Link element (Link8) was used for the tendons. Figure 4 shows the FE mesh of a girder. The mesh consisted of 8,452 elements and 11,620 nodes. The shear transfer coefficient for an open crack and a closed crack of Solid65 was 0.5 and 1.0, respectively. The boundary condition of the FE model was set as close as possible to the boundary condition of the test. The loads were applied to the top loading blocks as concentrated loads at the test load points. To model the boundary conditions associated with the bottom surface, the transversal displacement DOF associated with the nodes at the supports were restrained.

The compressive constitutive relationship proposed by Du (2014) [12] was adopted for concrete in the FE analyses, as shown in Eq. (1). The tensile constitutive relationship proposed by Du (2014) [12] was adopted, as shown in Eq. (2).

$$y=\begin{cases}1.2x-0.2x^6 & 0\le x<1\\ \dfrac{x}{10(x-1)^2+x} & 1\le x\end{cases} \quad (1)$$

$$y=\begin{cases}1.09x+0.82x^2-0.91x^3 & 0\le x<1\\ \dfrac{x}{5.5(x-1)^{1.9}+x} & 1\le x\end{cases} \quad (2)$$

in which, $x = \varepsilon / \varepsilon_0$, $y = \sigma / \sigma_0$, ε and σ are the strain and stress at the intersecting point of the first portion and the second portion on the stress-strain curve of the UHPC; ε_0 is the strain when the stress of the concrete reaches its peak value σ_0.

The elasto-plastic stress-strain curve was applied for the reinforcement, as shown in Eq. (3), while the stress-strain curve with no obvious plastic flow was used for external prestressed tendons, as shown in Eq. (4).

$$\sigma_y=\begin{cases}E_s\varepsilon & 0<\varepsilon\le\varepsilon_y\\ f_y & \varepsilon_y<\varepsilon\le\varepsilon_u\end{cases} \quad (3)$$

$$\sigma_p=\begin{cases}E_p\varepsilon_p & 0\le\varepsilon_p\le\varepsilon_{py}\\ f_{pk}+(\varepsilon_p-\varepsilon_{py})\dfrac{f_{pu}-f_{pk}}{\varepsilon_{pu}-\varepsilon_p} & \varepsilon_{py}\le\varepsilon_p\le\varepsilon_{pu}\end{cases} \quad (4)$$

in which, E_s and E_p are the elastic modulus of steel bar and prestressed tendons, respectively; ε_y and ε_{py} are elastic limit strain of steel bar and prestressed tendons, respectively; ε_u and ε_{pu} are hardening limit strain of steel bar and prestressed tendons, respectively; f_y and f_{pk} are yield stress of steel bar and prestressed tendons, respectively; f_{pu} is ultimate strength of prestressed tendons.

4. Test results and FE analysis

4.1 Deflection curves

The maximum longitudinal displacement of the girder was only 6.85 mm at the sliding bearings in test. It was indicated that the requirement as a simply-supported girder is satisfied. Figure 5 shows the load-versus-vertical-displacement curves of the model obtained from test and FE model. It can be seen that the structural behaviour of the girder can be divided into elastic phase, crack developing phase, and reinforcing steel yielding phase. For example, the mid-span of the model has the largest vertical displacement, in which the structural behaviour can be summarized as follows: 1) the girder is in elastic phase behaving linear elastically before the cracking; 2) the girder enters the crack developing phase after the first crack was observed at the bottom at 55 kN, and then the displacement increases nonlinearly; 3) the last phase begins when the reinforcing steel yields at the mid-span at 90 kN, and the displacement increases rapidly until the girder fails at 100 kN. It can be seen from Fig. 5 that good agreement is achieved between the test result and the FE prediction.

Figure 6 shows the model deflection curve in different loads. It can be seen that the curve of the girder subjected to symmetrical concentric loads is approximately symmetric.

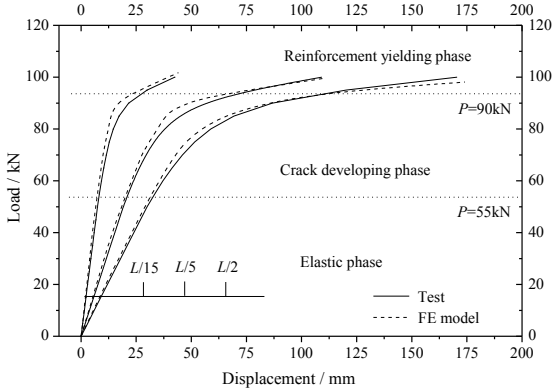

Fig. 5 – Load versus vertical displacements

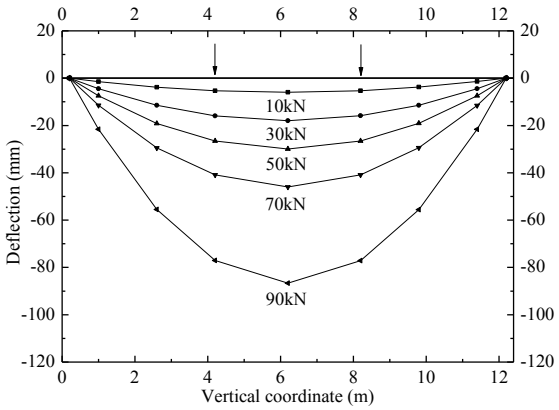

Fig. 6 – Deflection curves of the model

4.2 Cracks

The first crack appeared at mid-span while the load was increased to 55 kN. More cracks were observed with the increasing load. These cracks got wider and deeper and propagated towards lateral sides with further loading. The biggest crack width was about 0.6 mm, located at the bottom at the mid-span. The crack zone was about 5,750 mm long when the load was reached to 100 kN, as shown in Fig. 7(a). The crack distribution in the pure bending zone was uniform, with an average spacing of 95 mm. The cracks in the shear-bending zone were distributed in the range of about 900 mm from the load point. It is indicated that the anti-crack capaci-

ty of UHPC box girder is superior to that of normal precast concrete girder. The tensile strength of UHPC should be taken into consideration in the process of calculating the cracking moment.

The crack distribution of the FE model is within 6,447-mm length (see Fig. 7(b)), which is slightly larger than the test result. Therefore, the proposed numerical analysis approach can be employed to analyse well the mechanical behaviour of UHPC girders.

4.3 Strain distribution

The strain distribution of the test girder at mid-span is presented in Fig. 8(a). It can be seen that the average strain distribution of the girder agrees with plane section assumption. Figure 8(b) shows that the strains on concrete across the top flange are almost same: the difference between the maximum and the minimum is only 29 $\mu\varepsilon$. It shows that the strain distribution is relatively uniform on the flange and the shear lag effect is small in this kind of girder.

4.4 Failure mode

In the process of the experiment, there was no partial cracking and damage in wet joints. It is demonstrated that the construction method of the girder is feasible. The maximum compressive strain of UHPC is 744 $\mu\varepsilon$ in the test girder, smaller than the ultimate strain 3,373 $\mu\varepsilon$. The external prestressed tendons have not reached its ultimate strength when the girder damaged. The test girder demonstrated a ductile failure. Therefore, it is reasonable that the cross-section of test UHPC girder is under-reinforced as the normal PC beam for avoiding the brittle failure or even explosive destruction of UHPC.

4.5 Parametric studies

It has been shown in Section 4.1 that the FE can be used to model the UHPC girders with excellent accuracy. In order to compare the flexural behavior of UHPC girder with PC girder, the influencing parameter, i.e. concrete grade of C40, C60, and C80, with compressive strength of 40 MPa, 60 MPa, and 80 MPa, respectively, were studied numerically. Other geometric factors were kept the same as those in the test girder. The compressive and tensile stress-strain curves were modified for concrete grade of C40, C60, and C80, as shown in Eqs. (5) and (6), respectively.

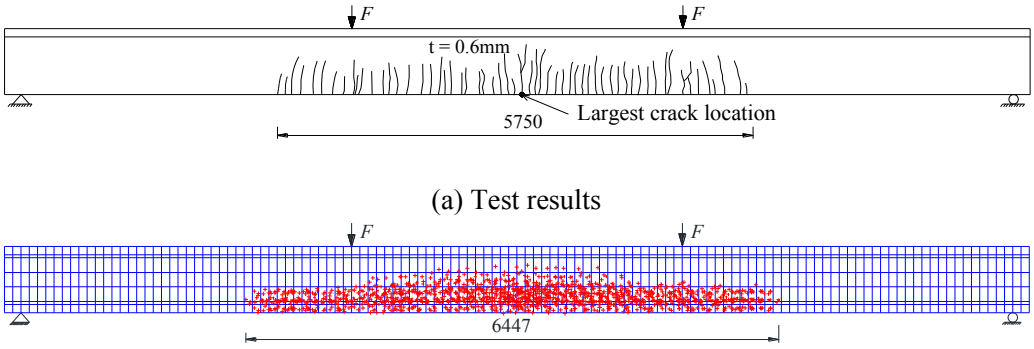

(a) Test results

(b) FE results

Fig. 7 – Crack distributions (unit: mm)

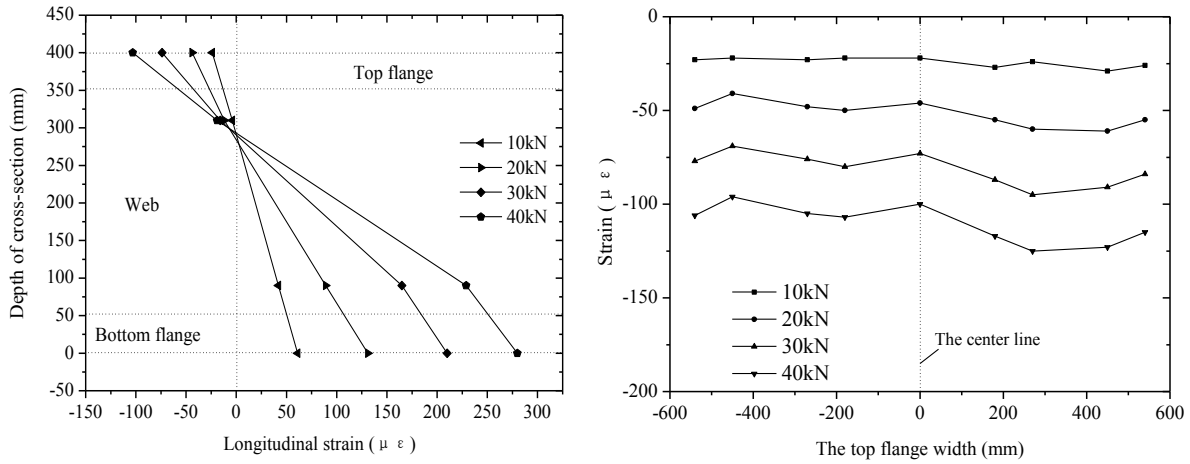

(a) Along the section depth

(b) Along the top flange

Fig. 8 – Strain distribution at mid-span

$$\sigma = \begin{cases} \sigma_0 \left[2\dfrac{\varepsilon}{\varepsilon_0} - \left(\dfrac{\varepsilon}{\varepsilon_0} \right)^2 \right] & 0 < \varepsilon < \varepsilon_0 \\ \sigma_0 \left[1 - 0.15 \left(\dfrac{\varepsilon - \varepsilon_0}{\varepsilon_{cu} - \varepsilon_0} \right) \right] & \varepsilon_0 < \varepsilon < \varepsilon_{cu} \end{cases} \quad (5)$$

$$\sigma = \begin{cases} \dfrac{\sigma_t}{\varepsilon_t} \varepsilon & 0 < \varepsilon \le \varepsilon_t \\ \sigma_t \dfrac{\varepsilon_{tu} - \varepsilon}{\varepsilon_{tu} - \varepsilon_t} & \varepsilon_t < \varepsilon \le \varepsilon_{tu} \end{cases} \quad (6)$$

in which, ε_{cu} and ε_{tu} are elastic limit strain and hardening limit strain of concrete, respectively.

Figure 9 shows the load-deflection relationship of different girders with different concrete grades at mid-span. The bending behaviour and failure mode of PC girders have three different stages of elastic stage, crack development stage, and failure stage, which is similar to that of test UHPC girder. However, the cracking load, reinforcement yield load, and ultimate load of UHPC girder are 34.1%, 34.3%, and 35.1% higher than those of PC girders (see Table 3). It is indicated that the compressive strength has less effect on the cracking, yield, and failure loads, while tensile strength of UHPC has better effect on those loads. Therefore, the tensile property of UHPC should be taken into account in the process of calculating mid-span nominal capacities of the externally prestressed UHPC box girder.

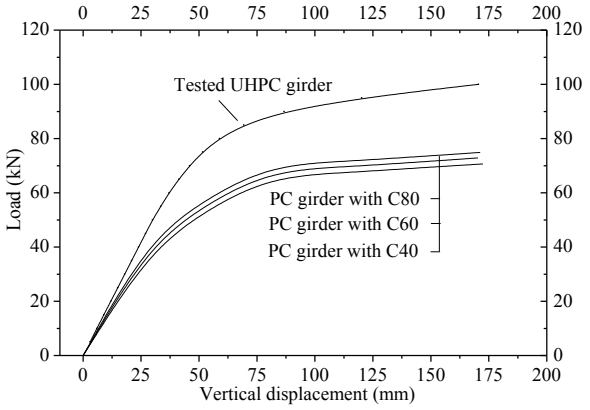

Fig. 9 – Load-deflection relationship of different girders at mid-span

Table 3 – Principal loads of different girders

Concrete grade	PC girder			Test UHPC girder
	C40	C60	C80	
Cracking load (kN)	40	41	42	55
Yield load (kN)	66	67	68	90
Failure load (kN)	73	74	75	100

5. Simplified calculation method of UHPC girder

5.1 Cracking moments

The distribution and simplified assumption of stress and strain of normal section when the girder began to crack is shown in Fig. 10. It assumes the stress of concrete in both of the compressive and tensile zones is equivalent to a triangle. Equations (7) and (8) can be obtained according to the equilibrium condition. y_t is the distance between the resultant forces of UHPC compressive and tensile zones, while y_s and y_p is the distance between the resultant forces of UHPC compressive zone with the resultant forces of steel bars and prestressed tendons, respectively. Table 4 lists the ultimate load of both simplified calculation and test results of the girder, as well as those of specimens in Ref. [13]. Based on the results, it can be found that the results are very close. In Table 4, the values of M_{cr}/ M'_{cr} are close to unity.

$$\int_{A_c} \sigma_c dA_c = \int_{A_t} \sigma_t dA_t + \sigma_y A_s + \sigma_p A_p \quad (7)$$

$$M_{cr} = \int_{A_t} \sigma_t y_t dA_t + \sigma_y A_s y_s + \sigma_p A_p y_p \quad (8)$$

in which, σ_c and σ_t are compression stress and tensile stress of UHPC, respectively; σ_y and σ_p are stress of steel bar and prestressed tendons, respectively; A_c and A_t are area of compressive zone and tensile zone of UHPC, respectively; y_t , y_s, and y_p are distance from the resulting force location of compressive zone to the resulting force location of tensile zone, steel bar, and prestressed tendons, respectively.

5.2 Ultimate load-carrying capacity

The distribution and simplified assumption of stress and strain of normal section at ultimate are shown in Fig. 11. It assumes the stress of concrete

in the compressive zone as a triangle, while the stress in the tensile zone is equivalent to a rectangle. It is taken as the ultimate tensile strength f_t multiplied by a reduction factor β. Equations (9) and (10) can be obtained according to the equilibrium condition. Table 5 lists the mid-span nominal bending capacity under different reduction factor. It can be found that the value of M_{u2}/M_{u1} is 0.96 when β = 0.8. Therefore, the simplified method coincided with test ultimate load better and safer, which was suggested for further use in practice.

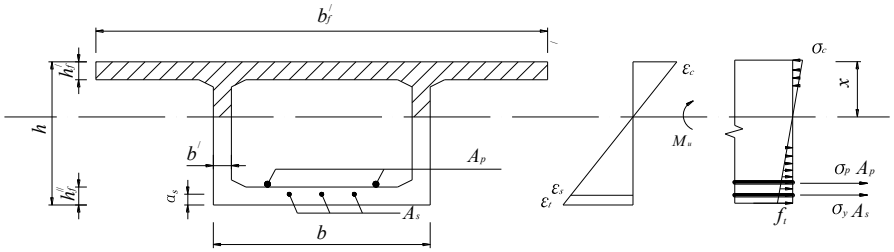

(a) Cross section (b) Strain (c) Stress

Fig. 10 – Schematic diagram of cracking moments of UHPC box girder

$$\int_{A_c} \sigma_c dA_c = \int_{A_t} \beta f_t dA_t + f_y A_s + \sigma_{pu} A_p \quad (9)$$

$$M_u = \int_{A_t} \beta f_t y_t dA_t + f_y A_s y_s + \sigma_{pu} A_p y_p \quad (10)$$

in which, σ_{pu} is ultimate tensile strength of prestressed tendons.

Table 4 – Comparison between calculation and test results

Item	Calculation M_{cr} (kN.m)	Test results M'_{cr} (kN.m)	M_{cr}/M'_{cr}
Test UHPC girder	125	130	0.96
UHPC girder (T600S) in Ref. [13]	212	224	0.95
UHPC girder (T1300S) in Ref. [13]	923	1011	0.91

Table 5 – Mid-span nominal bending capacity under different β

Reduction factor β	0.7	0.8	0.9	1
Test result M_{u1} (kN.m)	220	220	220	220
Calculation M_{u2} (kN.m)	202	211	221	230
M_{u2}/M_{u1}	0.92	0.96	1.00	1.05

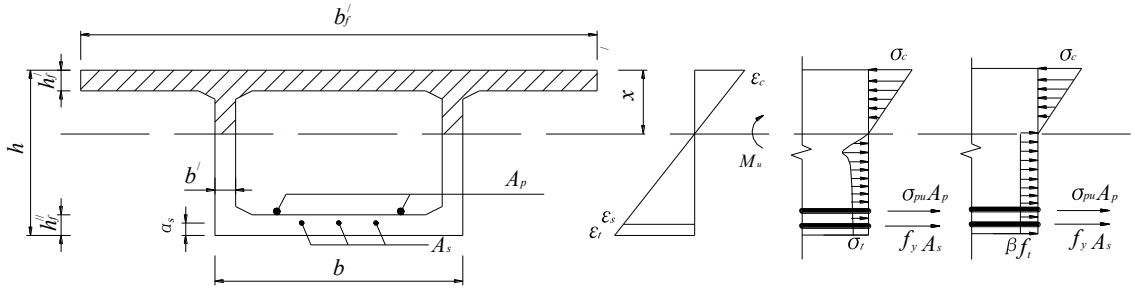

(a) Cross section (b) Strain (c) Stress (d) Equivalent stress

Fig. 11 – Simplified model at ultimate

6. Conclusions

In the process of the experiment, there is not partial cracking and damage in wet joints, which is demonstrated that the construction method of the girder is feasible. The girder presented ductile failure like the normal under-reinforced beam. The tensile strength of UHPC should be taken into account

in the process of calculating cracking moment and ultimate loads. Same as PC girder, the plane-section assumption is satisfied and can be used for sectional analysis in the test girder. The shear lag effect is small at the elastic stage in the girder, for it has just a little difference among the strains on the top flange at the mid-span. FE model analysis results agree well with the test results. The simplified cracking moment and ultimate load calculation method is proposed for the prestressed UHPC girder. It is demonstrated that the method can meets precision for practice engineering and can be a reference method for design calculation of a prestressed UHPC box girder.

Acknowledgment

This work was supported by the National Science Foundation under Grant No.U1305245, and Research Grant of the Fuzhou University (Project No. 510251) and the Education Department of Fujian Province (Project No. 601705).

References

1. Wang, D.H.; Shi, C.J.; Wu, Z.M.; Xiao, J.F.; Huang, Z.Y.; and Fang, Z. (2015) "A review on ultra high performance concrete: Part II. Hydration, microstructure and properties," Construction and Building Materials, 96, pp. 368-377.
2. Chen, B.C.; Šavor, Z.; Su, J.Z.; and Huang, Q.W. (2016) "A state-of-the-art of ultra-high performance concrete arch bridges," 1st International Conference on UHPC Materials and Structures, Hunan University, pp. 614-618.
3. Russell, H.G.; and Graybeal, B.A. (2013) "Ultra-High Performance Concrete: A State-of-the-Art Report for Bridge Community," U.S. Federal Highway Administration, Publication No. FHWA-HRT-13-060.
4. Tanaka, Y.; Maekawa, K.; Kameyama, Y. (2009) "Innovation and application of UFC bridges in Japan," Proceedings of UHPC 2009. Marseille, France, pp. 112-120.
5. Zimmermann, W. (2008) "UHPC – First applications with ultra high performance concrete in Austria," Proceedings of 4th Central European Congress on Concrete Engineering, Opatija, Croatia, pp. 184-194.
6. Zimmermann, W. (2009) "Construction method of 'Wild bridge völkermarkt," Austrian Society for Concrete and Construction Technology, Proceedings of 5th Central European Congress on Concrete Engineering, Baden, Austria, pp. 41-45.
7. Voo, Y.L.; Foster, S.J.; Faiz, M.; and Hassan, A. (2014) "The current state of art of ultra-high performance concrete bridge construction in Malaysia," Proceedings of the 12th International Conference on Concrete Engineering and Technology, 12-14 Aug., Selangor, Malaysia, pp. 95-102.
8. Voo, Y.L.; Foster, S.J.; and Voo, C.C. (2015) "Ultra-high performance concrete segmental bridge technology: toward sustainable bridge construction," Journal of Bridge Engineering, SPECIAL ISSUE: Design, Analysis, and Construction of Segmental Bridges, 20(8), B5014001.
9. Graybeal, B.A. (2008) "Flexural Behavior of an Ultra high-Performance Concrete I-Girder," Journal of Bridge Engineering, 13(6), pp. 602-610.
10. Yang, I.H.; Joh, C.B.; and Kim, B.S. (2011) "Flexural strength of large-scale ultra high performance concrete prestressed T-beams," Canadian Journal of Civil Engineering, 38(11), pp. 1185-1195.
11. Huang, Q.W.; Wu, Y.Y.; Du, R.Y.; Chen, B.C.; Chen, Y.Y.; and Wu, Q.X. (2012) "Trial-design Research on Reactive Powder Concrete Pedestrian Bridge," Journal of Fuzhou University (Natural Science edition), 37(4), pp. 751-756.
12. Du, R.Y. (2014) "Research on Ultimate Load-Carrying Capacities of Reactive Powder Concrete (RPC) Box Girder and Arch," Ph.D. Thesis, Fuzhou University.
13. Yang, J.; and Fang, Z. (2009) "Research on flexural behaviors of prestressed ultra high performance concrete beams," China Journal of Highway and Transport, 22(1), pp. 39-46.